Mon. Not. R. Astron. Soc. **329,** 290–300 (2002)

The metallicity of CM Draconis

Serena Viti,[1]★ Hugh R. A. Jones,[2] Pierre Maxted[3] and Jonathan Tennyson[1]
[1]*Department of Physics and Astronomy, University College London, Gower Street, London WC1E 6BT*
[2]*Astrophysics Research Institute, Liverpool John Moores University, Twelve Quays House, Egerton Wharf, Birkenhead CH41 1LD*
[3]*Department of Physics and Astronomy, University of Southampton, Highfield, Southampton S017 1BJ*

Accepted 2001 September 7. Received 2001 September 6; in original form 2001 May 2

ABSTRACT

We compare observations of the eclipsing binary system CM Draconis (hereafter CM Dra) with synthetic spectra computed using the stellar atmosphere code PHOENIX. High-resolution infrared spectroscopic observations of six 0.05-μm-wide regions between 1.51 and 2.45 μm, combined with previous work, particularly CM Dra's accurately known surface gravity, enable us to estimate its metallicity using detailed spectral synthesis. We find significant discrepancies between the observed and synthetic spectra throughout most of the region emphasizing the need for higher quality atomic data in the infrared. Nevertheless, the $\Delta\nu = 2$ CO bands beyond 2.3 μm seem to be well modelled and metal-sensitive, and thus high-resolution spectra should be a most powerful diagnostic tool for spectroscopic analyses for M dwarfs and brown dwarfs. The CO bands indicate a metallicity of around −1 dex for CM Dra. This result is supported by observations of two M dwarfs of similar spectral type, GJ 699 (Barnard's star) and GJ 725B. This result supports inferences from previous infrared work, although it does not agree with standard evolutionary models or optical analyses, which both suggest an abundance for CM Dra close to that of the Sun.

Key words: stars: atmospheres – binaries: eclipsing – stars: fundamental parameters – stars: late-type – stars: low-mass, brown dwarfs – stars: Population II.

1 INTRODUCTION

Low-mass stars are the most dominant objects in our Galaxy in terms of number density. They provide a probe of our understanding of main-sequence stellar evolution, and are the key in determining the boundary between stellar and substellar objects. There are relatively few observations of low-mass stars with known masses. Parameters such as effective temperatures and metallicities, vital in determining positions in HR diagrams, remain controversial. To reliably constrain the low-mass initial stellar mass function, it is essential to know the basic properties of standard low-mass M, L and T dwarfs. A correct determination of the mass function relies on an accurate transformation from luminosity and temperature to mass. This relationship is very sensitive to the stellar chemical composition (e.g. Fig. 1). Usually, colour–colour diagrams are used as indicators of metallicity. However, these diagrams, constructed with evolutionary and atmospheric models, do not yet reproduce the broad-band fluxes within a reasonable error, and therefore cannot be uniquely used to determine metallicities (Fig. 1).

A number of authors have determined metallicities spectroscopically by comparing with synthetic spectra. However, such synthetic spectra are problematic because (1) the objects are dominated by various diatomic and triatomic molecules whose properties are poorly understood, and (2) the large number of different transitions means that most transitions are substantially blended with other competing opacities. The most compelling investigations of low-mass metallicity are by Bessell (1982) and Gizis (1997), who have found CaH:TiO band strength indicators in the 6700–7000 Å region that have allowed discrimination of M dwarfs into three categories: disc-like; intermediate-band strength subdwarfs, class sdM; and extreme subdwarfs, class esdM. Synthetic spectra and the use of higher mass companions suggest preliminary average metal abundances of [M/H] ≈ -2 for the esdM dwarfs, and [M/H] ≈ -1.3 for the sdMs. Although this provides a powerful empirical technique, it (1) is not sufficiently sensitive to distinguish mildly metal-poor stars, (2) relies on accurate synthetic spectra in a region with many transitions, particularly the poorly modelled molecules CaH and TiO, and (3) is not extendable into the brown dwarf regime.

Alternatively, spectral analysis of a large number of features can be used: Viti et al. (1997) attempted to derive the metallicity of the well-known eclipsing binary CM Draconis (hereafter, CM Dra) by comparing selected atomic features of its infrared and optical spectra with synthetic spectra. However, the relatively low resolution of their observations (∼800) meant that blending

★E-mail: sv@star.ucl.ac.uk

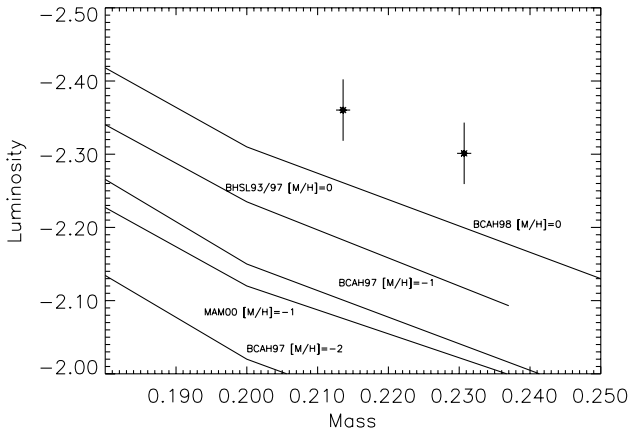

Figure 1. Points indicate two components of CM Dra system. Solid lines show different available model calculations: Burrows et al. (1993, 1997) denoted by BHSL, Baraffe et al. (1997, 1998) denoted by BCAH, and also model calculations from Montalban, D'Antona & Mazzitelli (2000) denoted by MAM00.

affected the individual atomic lines and molecular bands, leading to a number of uncertainties in the reliability of model comparisons.

CM Dra is the lowest mass main-sequence eclipsing binary known (RA $= 16^{\rm h}34^{\rm m}24^{\rm s}$, Dec. $= 57°09'00''$J2000, $V = 12.9$). Lacy (1977) first determined accurate masses and radii for CM Dra and suggested that its large space velocity ($163\,{\rm km\,s^{-1}}$) and low flaring rate mean that it could belong to Population II. This led Paczyński & Sienkiewicz (1984) to point out that if CM Dra were from Population II it would be an important system for cosmology, because its initial helium abundance can be determined from models of its structure. Because it is one of the faintest, smallest and least massive eclipsing main-sequence binaries so far known, its properties are of prime importance in understanding the properties of stars near the bottom of the main sequence.

Some of the fundamental physical properties of the components of CM Dra have already been determined accurately. Most important are the masses of $M_{\rm A} = 0.2307 \pm 0.0010$ and $M_{\rm B} = 0.2136 \pm 0.0010\,{\rm M}_{\odot}$, radii of $R_{\rm A} = 0.2516 \pm 0.0020$ and $R_{\rm B} = 0.2347 \pm 0.0019 R_{\odot}$ (Metcalfe et al. 1996), luminosities $L_{\rm A} = (4.998 \pm 0.504) \times 10^{-3}\,{\rm L}_{\odot}$ and $L_{\rm B} = (4.362 \pm 0.441) \times 10^{-3}\,{\rm L}_{\odot}$ (Viti et al. 1997), and surface gravities of $\log g = 4.999 \pm 0.007$ for CM Dra A and $\log g = 5.028 \pm 0.007$ for CM Dra B (Jones et al. 1996). The luminosities, radii and distance of the system suggest temperatures of close to 3100 K, although infrared spectroscopic analysis indicates somewhat higher temperatures (Viti et al. 1997). The precision of the above values far exceeds those known for any other M dwarf, and means that CM Dra is an excellent system for comparison with model calculations. This gave us the motivation to obtain high-resolution infrared spectra in order to investigate the metallicity of the system and make the first observations of M dwarfs in the infrared at high spectral resolution.

CM Dra's high space velocity and low flaring rate have led to the general assumption that it belongs to Population II. Rucinski (1978) intercompared optical Mg, MgH and TiO features of CM Dra with six other M dwarfs and concluded that it may be a subdwarf, but noted that the reliability of the determination is low. Gizis (1997) classified spectroscopically a series of M dwarfs and M subdwarfs, and found CM Dra to have a solar metallicity using spectra from 0.62 to 0.74 μm; Leggett, Allard & Hauschildt (1998) came to a similar conclusion based on comparisons between observed infrared and synthetic colours, although they noted significant discrepancies in the metallicity indicated by different colours. Viti et al. (1997) investigated spectra from 0.4 to 2.4 μm, and found discrepancies between the analysis of the infrared and optical spectra: while the optical spectral energy distribution (SED) yields a metal-rich solution with $T_{\rm eff} = 3000$ K, the infrared SED yields $T_{\rm eff}$ around 3200 K with $-0.8 \leq {\rm [M/H]} \leq -0.6$ and suggests that CM Dra could be perhaps a chemically peculiar system.

Most of these analyses suffer from the problem that they are dependent on synthetic atmospheres whose primary opacities of TiO, metal hydrides and H_2O were relatively poorly modelled. Additionally, these poorly modelled opacities are blended in low-resolution observations. Thus Viti et al.'s (1997) approach of spectral analysis of individual spectroscopic features over a large wavelength range was hampered by relatively low resolution. None the less, this analysis indicated particular weak lines that might not be (1) overly influenced by poorly modelled opacities, (2) blended, and (3) subject to saturation effects and infilling from the chromosphere. In this paper we attempt to select a number of features based on the Viti et al.'s work and observe them at higher spectral resolution. The observations and models used are described in Sections 2 and 3. Sections 4 and 5 present the analysis and the results obtained.

Table 1. Central wavelengths and wavelength coverages, resolutions, dates of the observations, and integration times.

$\lambda_{\rm cen}$ μm	$\lambda_{\rm range}$ μm	Resolution μm	Date dd/mm/yy	Time (total) minutes
1.579	1.568–1.588	9846	14/06/97	5
1.596	1.585–1.607	9952	14/06/97	5
2.162	2.146–2.177	12594	14/06/97	5
2.187	2.172–2.201	12740	14/06/97	5
2.238	2.222–2.255	13037	16/06/97	5
2.313	2.298–2.326	13474	16/06/97	5

2 OBSERVATIONS

CM DraAB (GJ 630.1AB, LHS 421), spectral type M4.5V, $V - K = 5.1$, GJ 725B (LHS 59), spectral type M3.5V, $V - K = 4.71$, and GJ 699 (Barnard's star, LHS 57), spectral type M4V, $V - K = 5.04$, were observed on the nights of 1997 May 14 and 16 with the Cooled Grating Spectrometer 4 (CGS4, 2001) on the UK Infrared Telescope (UKIRT) on Mauna Kea, Hawaii.

At that time, CGS4 used a 256×256 InSb array. Comparison sky spectra were obtained by nodding the telescope so that the object was measured successively in two rows of the array, separated by 30 arcsec. The echelle grating ${\rm mm^{-1}}$ and short focal length (75 mm) was used with central grating wavelengths of 1.579, 1.596, 2.138, 2.162, 2.187, 2.238 and 2.313 μm. The wavelength coverage, resolutions and integration times of the observations are listed in Table 1, and the spectra of CM Dra are shown in Fig. 2. The grating positions were chosen from the features identified to be relatively metallicity-sensitive in Viti et al. (1997) and Viti & Jones (1999), although the availability of blocking filters and the desire not to work at high grating angles, where the efficiency drops dramatically, meant that we were quite restricted in the choice of wavelength.

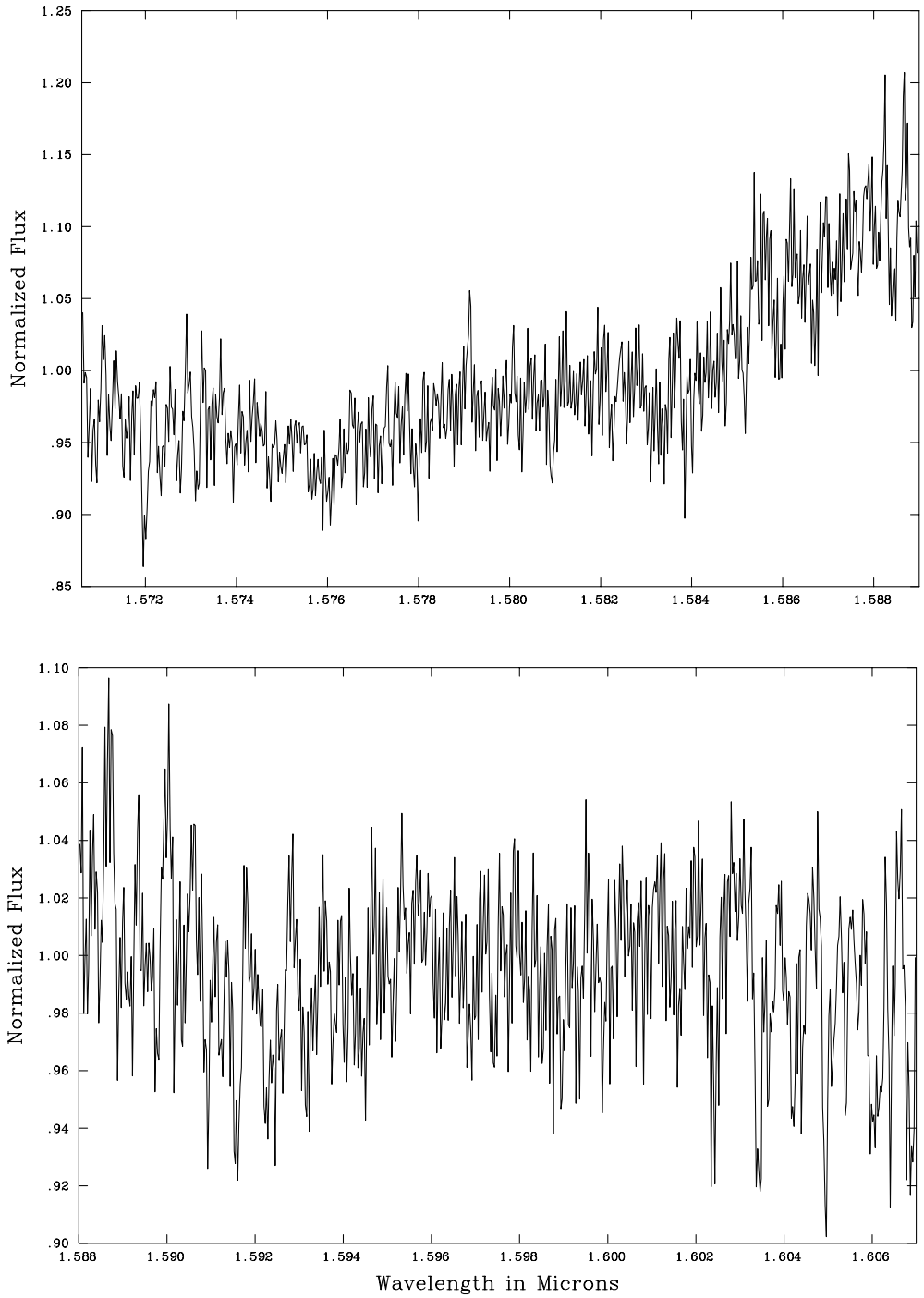

Figure 2. Spectra for CM Draconis: (a) 1.579 μm – orbital phase of 0.223, (b) 1.596 μm – orbital phase of 0.205, (c) 2.138 μm – orbital phase of 0.195, (d) 2.162 μm – orbital phase of 1.00. Note that the large broad peak is due to uncorrected hydrogen line from standard star. (e) 2.187 μm – orbital phase of 0.280 (f) 2.238 μm – orbital phase of 0.00, (g) 2.313 μm – orbital phase of 0.240. Note that the efficiency of each grating cuts off dramatically at the ends.

To remove telluric bands of water, oxygen, carbon dioxide and methane, we observed an A2p star, SAO 29931, and used it as a standard. Such stars are not expected to have features in common with stars like CM Dra, and are mainly featureless except for some hydrogen lines. The airmass difference between object and standard used never exceeded 0.05, and so we are confident that the spectra have good cancellation of atmospheric features, although in some spectra, hydrogen lines have been introduced into the spectrum when dividing by the standard. Both the object and the standard were wavelength-calibrated by using arc lines of krypton, argon and xenon, and OH lines. The accuracy of the calibration is quite poor and variable due to the lack of available arc lines. The sky subtraction was obtained with standard routines which eliminate any residual sky emission due to the variance of sky brightness between object and sky pairs. The signal was spread between three rows. To extract the spectrum from the sky-subtracted signal an optimal extraction technique (Horne 1986) was used; this combines the rows using weights based on the spatial profile of

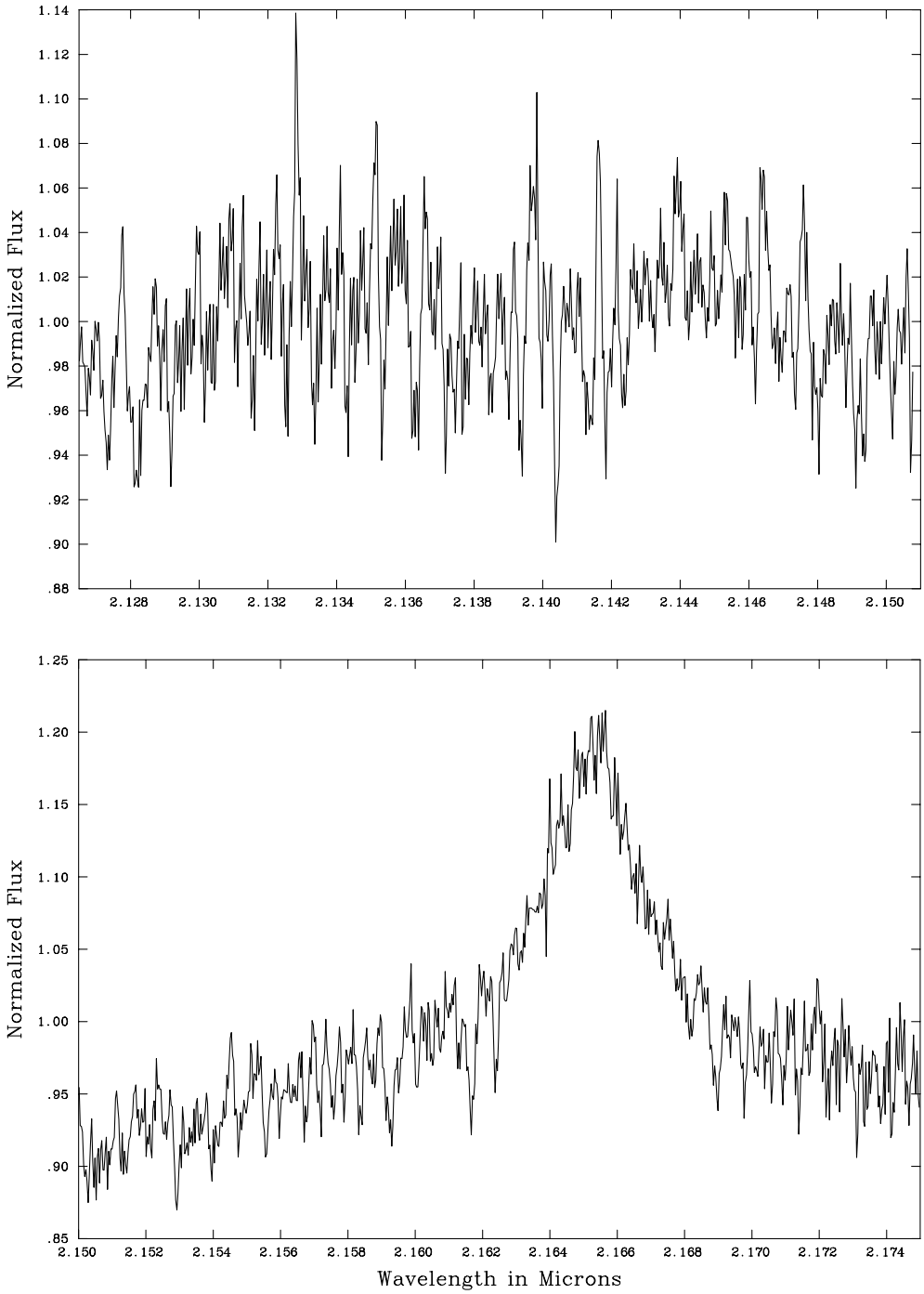

Figure 2 – *continued*

the stellar image. The spectra were reduced by using the FIGARO, SPECDRE and KAPPA packages provided and supported by Starlink.

Our spectroscopic measurements of CM Dra were made at various phases. We calculated the phase of the system during our observations based on fig. 2 from Metcalfe et al. (1996), and include these values in the caption for Fig. 2. Rather than having composite spectra consisting of different spectral regions having different relative contributions from the A and B components, we chose one observation per spectral region. Our choice was based on two criteria: (1) the best S/N spectrum, and (2) the one with a phase closer to an eclipse. The components are measured to have a similar temperature (within 100 K), and the phase information is primarily important to understand the broadening of features due to the combined spectra. These observations were part of a larger data set intended to disentangle the spectra for each component of the CM Dra system at high resolution from 0.4 to 2.5 μm (Maxted, Viti & Jones, in preparation).

3 THE MODELS

Model spectra were computed for this project with the model atmosphere code PHOENIX using the version known as NextGen

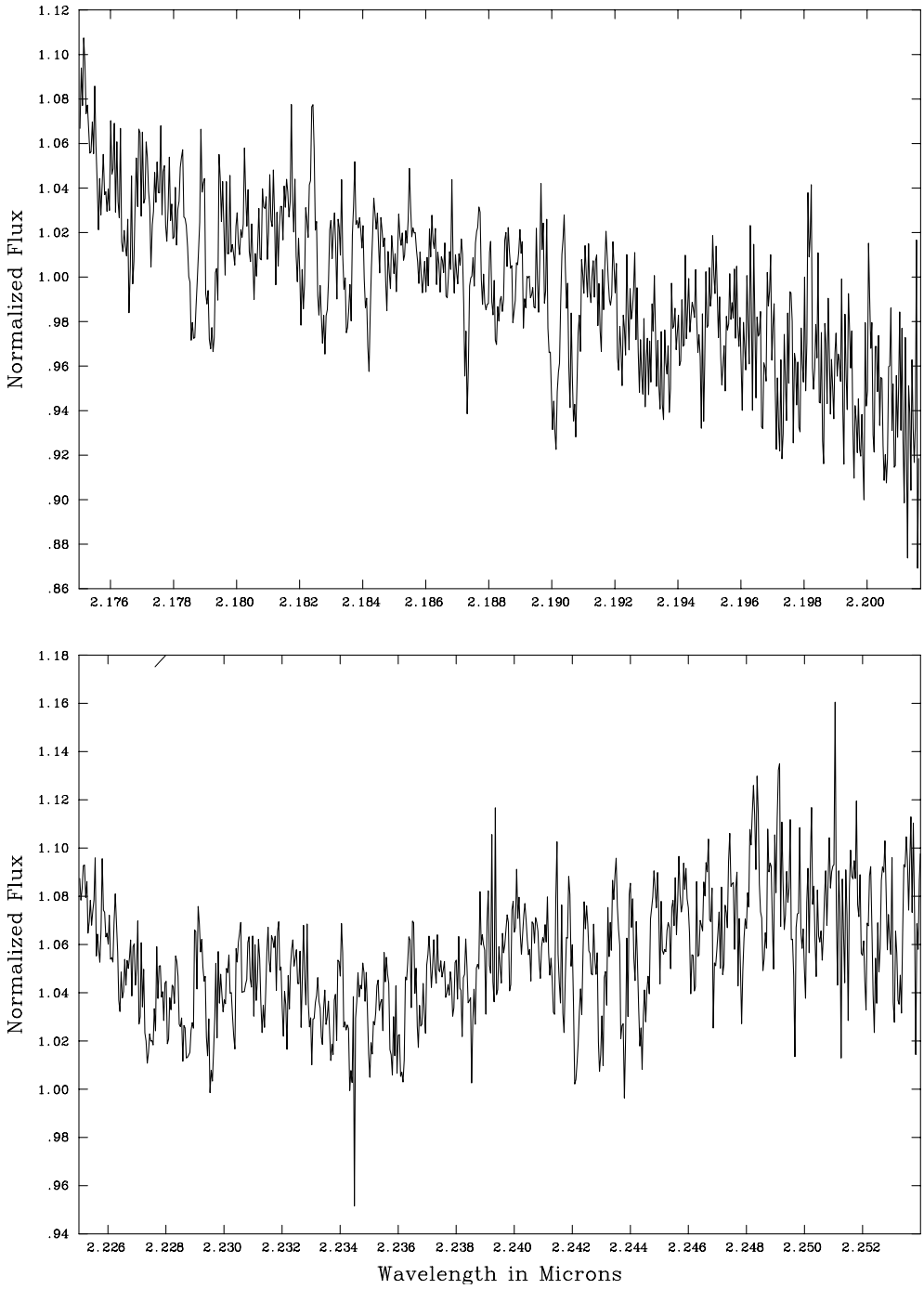

Figure 2 – *continued*

(Hauschildt, Allard & Baron 1999). Log $g = 5.0$ is adopted for all models, since the surface gravity of the CM Dra pair is close to $\log g = 5.0$ with a small error. Model temperatures of 3100 to 3300 K and metallicities from [M/H] $= -1.0$ to 0.0 are investigated in this work. These parameters represent the probable extremes of metallicity and effective temperature of CM Dra based on previous work. We have not tried comparing the system with models computed with non-solar abundance patterns.

Different features show very different dependencies on adopted temperature and metallicity. In Figs 3 and 4 we investigate the sensitivity of an example atomic feature and of CO bands respectively to changes in temperature and metallicity. The top panels of Figs 3 and 4 show the ratio of two models which differ only in metallicity, and the bottom panels show the ratio of two models which differ only in effective temperature. Models have been normalized to have the same mean value and the same y-scale is adopted for all plots for consistency. Fig. 3 shows one of the atomic features (Si I) most sensitive to both metallicity and effective temperature. Although in Fig. 3 we show the sensitivity of the models in only a small region, we have repeated this analysis for other regions where atomic opacity dominates. Moreover,

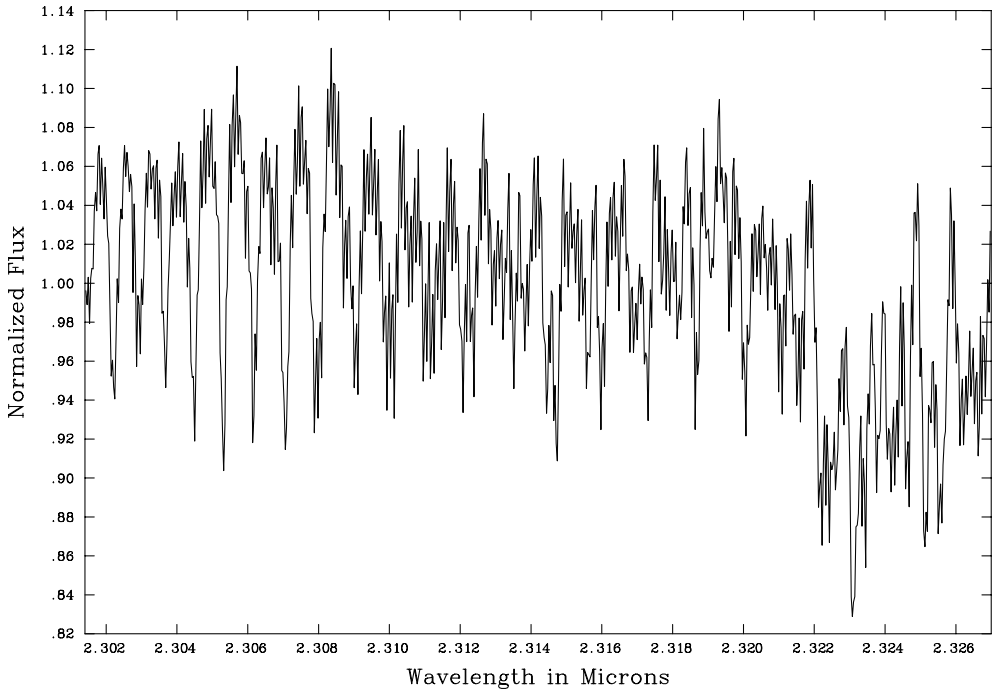

Figure 2 – *continued*

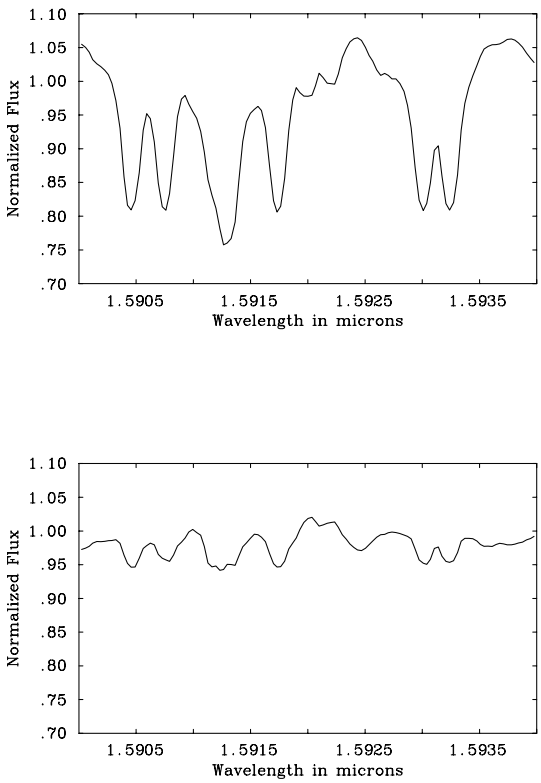

Figure 3. Sensitivity of the models to changes in $T_{\rm eff}$ and [M/H] for a selected region. Top: division of [M/H] = 0.0 with [M/H] = −1.0, both with a temperature $T_{\rm eff} = 3100$ K. Bottom: division of the $T_{\rm eff} = 3100$ K model with the $T_{\rm eff} = 3300$ K, both with metallicities of [M/H] = 0.0.

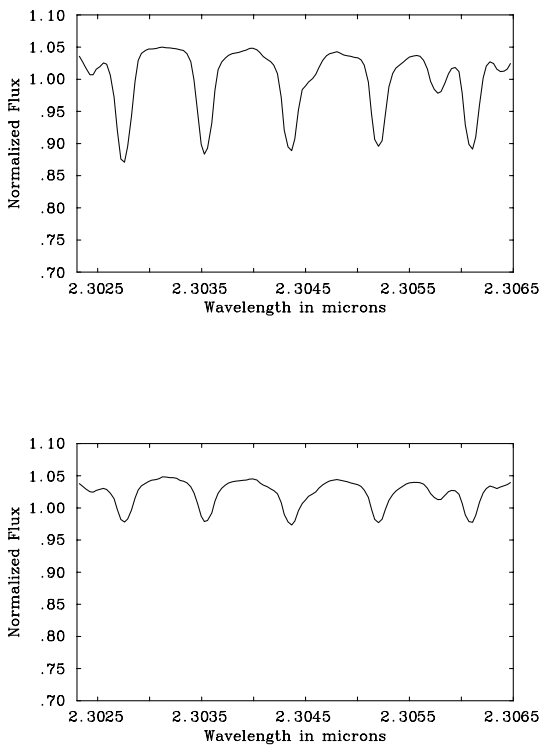

Figure 4. Sensitivity of the models to changes in $T_{\rm eff}$ and [M/H] across the CO bands $\Delta\nu = 2$. Top: division of [M/H] = 0.0 with [M/H] = −1.0, both with a temperature $T_{\rm eff} = 3100$ K. Bottom: division of the $T_{\rm eff} = 3100$ K model with the $T_{\rm eff} = 3300$ K, both with metallicities of [M/H] = 0.0.

Figs 3 and 4 show that a change in metallicity rather than temperature causes a greater change in the strength of the atomic lines and the CO bands. The resolution of the models in Figs 3 and 4 (and in most of the other figures) is reduced to match the observations by smoothing with a triangular function and resampling. This mimics the effect of detection by the rectangular pixels used by the detector and 3 times oversampling employed for the observations. The smoothing of the synthetic spectra was performed using routines within the KAPPA and SPECDRE packages

and spectral comparisons within the DIPSO. The analysis is divided in two sections: the atomic features and the CO bands.

After completion of this work, more recent model structures became available (e.g. Allard, Hauschildt & Schwenke 2000). We have therefore undertaken some tests with these latest models. In general, we find nothing that would alter the conclusions of this paper.

We have also investigated the effect of different mixing lengths by comparing models computed with an effective mixing-length parameter of 2.0 rather than 1.0 (as the 1999 NextGen synthetic spectra), and we found the differences to be negligible for the purpose of this paper.

4 SPECTROSCOPIC ANALYSIS

4.1 Atomic features

The analysis of Viti et al. (1997) investigated the SED of CM Dra, together with a wide range of spectral features. Despite the wide ranging nature of this investigation, the interpretation was affected by important caveats: (1) the completeness of H_2O and TiO for the SED, and (2) the lack of accurate oscillator strengths for the atomic transitions in the infrared.

Although we also found that low metallicity was the best fit in absolute terms, in common with the Viti et al. (1997) analysis, we generally found that the relative weakness of observed features meant that within our grid of models features were best fitted by models of higher temperature and higher metallicity, or lower temperature and lower metallicity. We have carefully examined the atomic and molecular features shown in Fig. 2. As suggested by the sensitivity plots (Figs 3 and 4), there are many features which are relatively sensitive to metallicity rather than temperature. However, in most cases it proved difficult to find a fit that we are confident with. For example, in Fig. 5 we show three metallicity-sensitive regions, and in Fig. 6 one temperature-sensitive region. Some of the lines were not easily identifiable using spectral atlases and the line ID feature within the synthetic spectral code PHOENIX. We expect that most of these are due to molecular features that have yet to be characterized. The continuous thick line is the CM Dra spectrum, while the continuous and the dotted thin lines in the top panels are models computed at [M/H] $= -1.0$ and 0.0 respectively, and $T_{\rm eff} = 3100$ K. Note that we have applied a velocity shift to the models in order to correct for the radial velocity of the CM Dra system at the observed phases. Therefore, for example, the Si line at $\sim$1.5931 μm (as in Fig. 3) appears at $\sim$1.5925 μm. In Fig. 6, again, the continuous thick line is the CM Dra spectrum, while the continuous and the dotted thin lines are models computed respectively at $T_{\rm eff} = 3300$ and 3100 K; both models are at [M/H] $= -1.0$. Apart from noticing from Fig. 5 and other similar plots that the low-metallicity models provide better fits, we are unable to draw any robust conclusions from these comparisons. Our investigation of atomic transitions suffers from the same problems as Viti et al. (1997). On the other hand, this is not the case for the CO bands.

4.2 CO bands

In the spectral region between 2.29 and 2.45 μm, CO dominates the

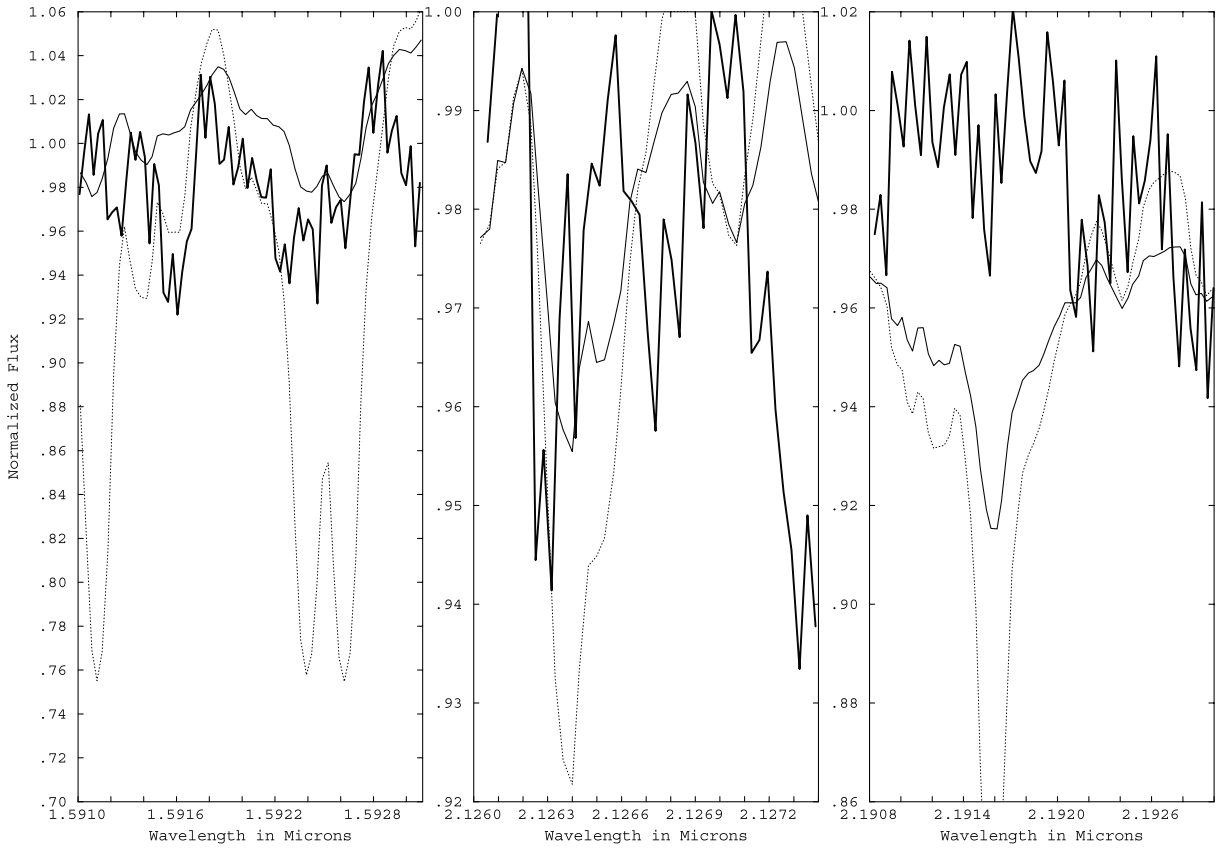

Figure 5. Spectra for CM Draconis compared with synthetic spectra for specific features of interest. Thick continuous line: CM Dra; thin continuous line: 3100 K, [M/H] $= -1.0$ model; dotted line: 3100 K, [M/H] $= 0.0$ model. The strong atomic features on the left, centre and right panels are Si I ($\sim$1.5931 μm shifted to $\sim$1.5925 μm), Al I ($\sim$2.1272 μm shifted to $\sim$2.1264 μm) and Ti I ($\sim$2.1925 μm shifted to $\sim$2.1916 μm).

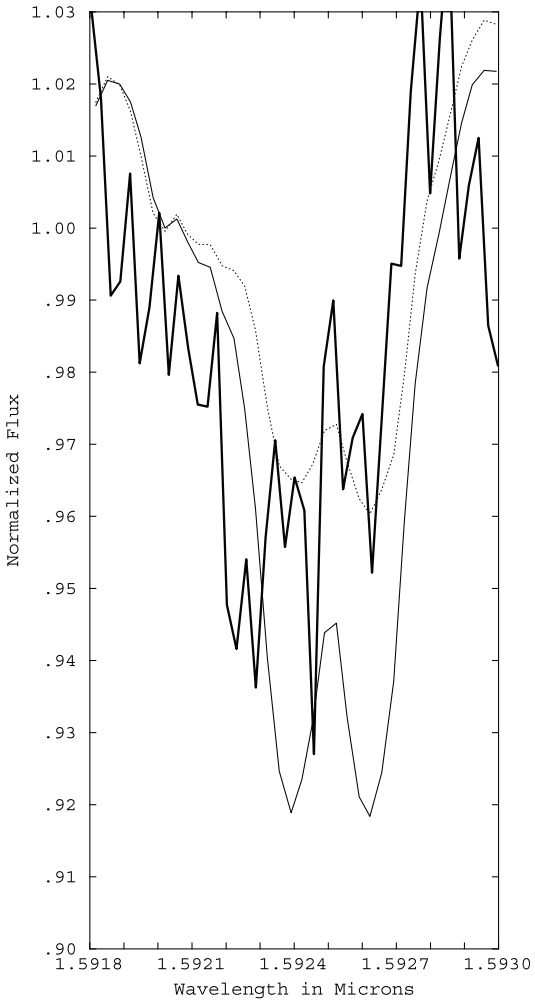

Figure 6. Spectrum for CM Dra compared with synthetic spectra for specific features of interest. Thick continuous line: CM Dra; thin continuous line: 3100 K, [M/H] = −1.0 model; dotted line: 3300 K, [M/H] = −1.0 model. The atomic feature is Si I (∼1.5931 μm shifted to ∼ 1.5925 μm).

Table 2. List of CO transitions from 2.29 to 2.32 μm. The wavelength in μm is listed in the first column, the lower energy level in K is listed in the second column, and the lower rotational quantum number is listed in the third column.

λ (μm)	E'' (K)	R
2.3005	2913.65	R32
2.3005	13166.85	R69
2.3013	2737.62	R31
2.3013	13542.42	R70
2.3021	2567.03	R30
2.3021	13923.01	R71
2.3030	2401.87	R29
2.3030	14308.60	R72
2.3039	2242.16	R28
2.3039	14699.17	R73
2.3048	2087.90	R27
2.3049	15094.72	R74
2.3058	1939.10	R26
2.3059	15495.23	R75
2.3068	1795.76	R25
2.3069	15900.67	R76
2.3078	1657.89	R24
2.3080	16311.05	R77
2.3089	1525.49	R23
2.3092	16726.33	R78
2.3101	1398.57	R22
2.3103	17146.51	R79
2.3112	1277.13	R21
2.3116	17571.56	R80
2.3125	1161.19	R20
2.3128	18001.48	R81
2.3137	1050.73	R19
2.3142	18436.24	R82
2.3150	945.77	R18
2.3155	18875.82	R83
2.3163	846.31	R17
2.3169	19320.22	R84
2.3177	752.36	R16
2.3184	19769.41	R85
2.3191	663.91	R15
2.3199	20223.38	R86
2.3206	580.98	R14

opacity of low-mass stars. CO appears in a relatively easily observed stable part of the *K* band, and molecular data, including *f*-values, are well known. Moreover, CO is believed to be formed under LTE (e.g. Carbon, Milkey & Heasley 1976), and therefore the levels are populated according to the Boltzmann distribution.

With an echelle spectrometer some individual rotational CO transitions can be resolved. In particular, the opacity between 2.29 and 2.32 μm is made up of a large number of spectral lines, covering a wide intensity range, of the second overtone of CO ($\nu = 2$–0). The second-overtone band of CO originates from vibration–rotation transitions in the ground electronic state $X\,^1\Sigma$, and obeys the selection rules $\Delta\nu = 2$ and $\Delta J = \pm 1$. The bandhead of the second overtone (i.e., the point at which the separation between the R transitions is zero) occurs at ∼2.290 μm, and therefore in the region of interest where one sees both 'hot' [such as R(80)] and 'cold' [such as R(20)] rotational transitions. Table 2 lists all the transitions present in the region 2.29–2.32 μm. Note that the $2J + 1$ statistical weight will act to increase the number density of high rotational levels, and so, though still following the Boltzmann distribution, the intensity difference between low and high *J* will not be as pronounced. We have chosen this region rather than the redder one (2.320–2.326 μm, $\nu = 3$–1) because (i) the latter region contains a large number of CO features very close together – at the resolution available to us, blending would then make spectroscopic analysis very difficult, and (ii) comparison of synthetic spectra show that the region between 2.29 and 2.32 μm is particularly insensitive to small temperature differences (∼200 K) (Fig. 3). The latter behaviour confirms findings by Kraus et al. (2000) which show that the synthetic spectra of the $\nu = 2$–0 bandhead emission, unlike other bandheads such as the $\nu = 3$–1, look very similar for temperatures in the range 3000–5000 K, although they did not explore lower temperatures. We also found this overtone to be particularly sensitive to metallicity (Fig. 4). It seems reasonable, therefore, to chose the second overtone of CO as a tracer of metallicity.

In fact, the second overtone of CO has been successfully used in the past as a tool to determine fundamental stellar parameters for M-giant stars (e.g. Tsuji 1986, 1991) and for the Sun (Tsuji 1977), but not for M dwarfs.

Because of the relative simplicity of the singlet sigma state, laboratory as well as theoretical analyses on the infrared spectrum of CO are well developed (e.g. Goorvitch 1994). Fig. 7 shows a high-resolution (0.05 Å) synthetic spectrum from 2.3035 to

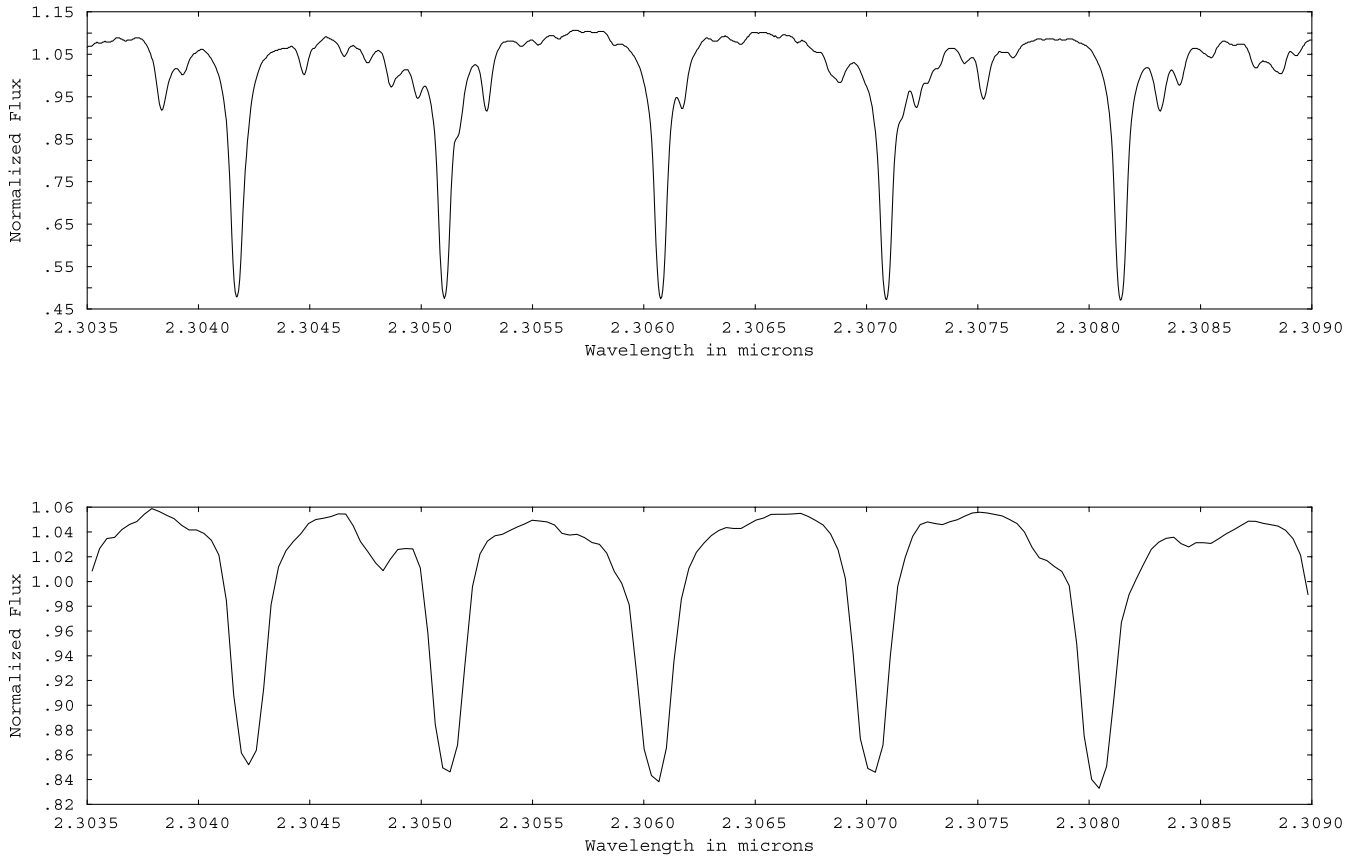

Figure 7. Top: high-resolution (0.05-Å) synthetic spectrum of the CO second overtone. Bottom: same as top but for lower resolution.

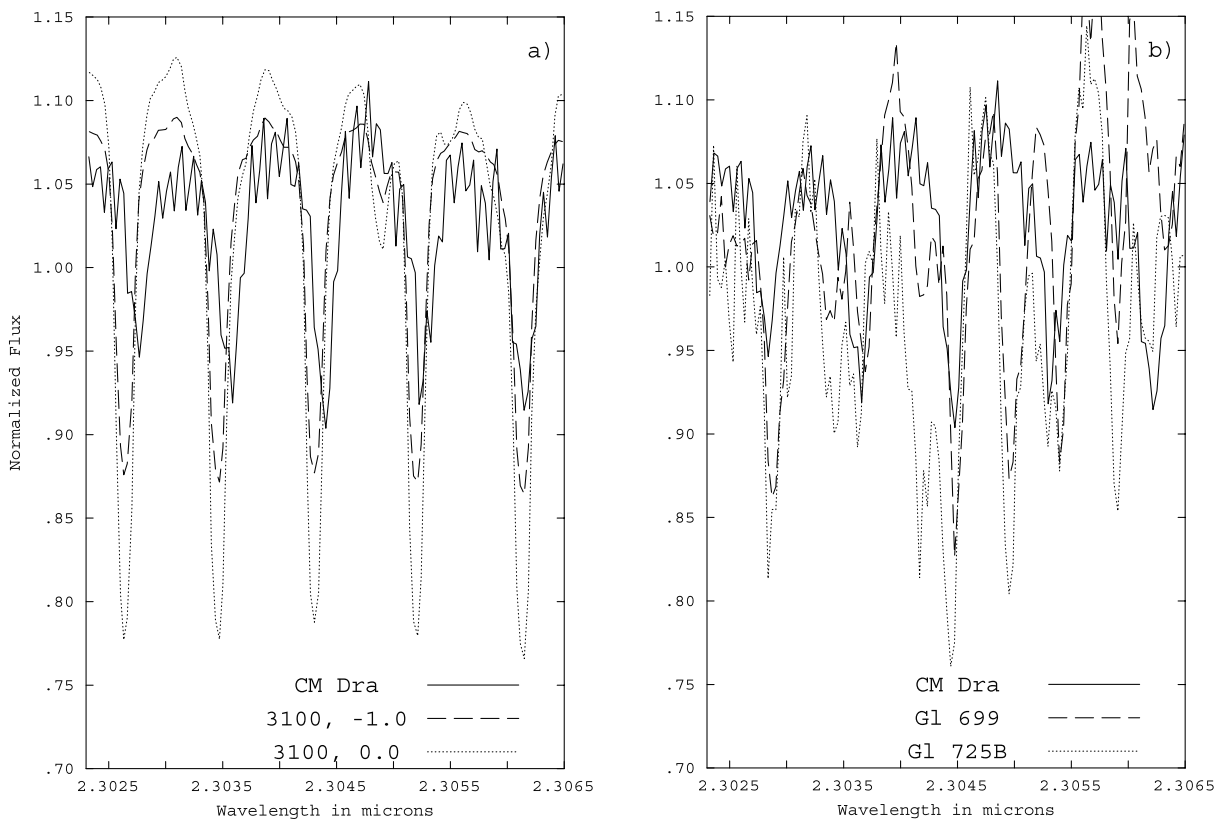

Figure 8. Carbon monoxide bands for CM Dra compared with synthetic spectra ($T_{\rm eff} = 3100$ K) (panel a) and with comparison stars (panel b).

2.3090 μm (top panel) and a synthetic spectrum in the same region but at the same resolution as the observations (bottom panel). From this figure it can be seen that weak lines, such as the ones belonging to the rotational transitions R75, R76 and R77, can be resolved if the resolution is at least 0.1 Å. In our observations these weak, high-energy bands are blended with the stronger ones. However, theoretical studies of the bandheads can help to understand the blending effects caused by the higher energy ones.

In contrast to the atomic features, we found a better match between observed and synthetic CO-band spectra. In Figs 8(a) and 9, we overplot the CO bands of CM Dra (continuous line) for two models differing in metallicity; the chosen models have been calculated at a fixed temperature of $T_{\rm eff} = 3100$ K (Fig. 8a) and $T_{\rm eff} = 3300$ K (Fig. 9). In both cases, the low-metallicity model is a much better match to the observed spectrum than the solar-metallicity one. We also compare CM Dra with GJ 699 and GJ 725B (Fig. 8b). Based on their colours and spectral types, both of these comparison objects are expected to be slightly hotter than CM Dra which, if they had the same [M/H], would lead them to have weaker CO bands. GJ 725B has slightly stronger CO bands than GJ 699, but both have substantially stronger bands than CM Dra. This is strong evidence that CM Dra is metal-poor relative to GJ 699 and GJ 725B. The spectra for GJ 699 and GJ 725B match the solar-metallicity models reasonably well, whereas the CM Dra spectrum is much closer to the model computed with [M/H] $= -1$. Previous analysis of both GJ 699 and GJ 725B indicate them to be metal-poor. GJ 699 is expected to have a metallicity close to [M/H] $= -0.5$ based on kinematic, photometric (Leggett 1992) and spectroscopic analysis (Jones et al. 1996), whereas based on high-resolution optical spectra GJ 725B has [M/H] $= -0.9$ (Valenti et al. 1998), although Leggett finds a solar-like [M/H]. Leggett indicates that GJ 699 is more metal-poor than GJ 752B, which is consistent with its stronger CO features in Fig. 8(b). Although the literature [M/H] values for GJ 699 and GJ 725B are wide ranging, it seems probable that they are both metal-poor. This strengthens our inference from Fig. 8(a) that CM Dra has a metallicity lower than -0.5, probably closer to -1.

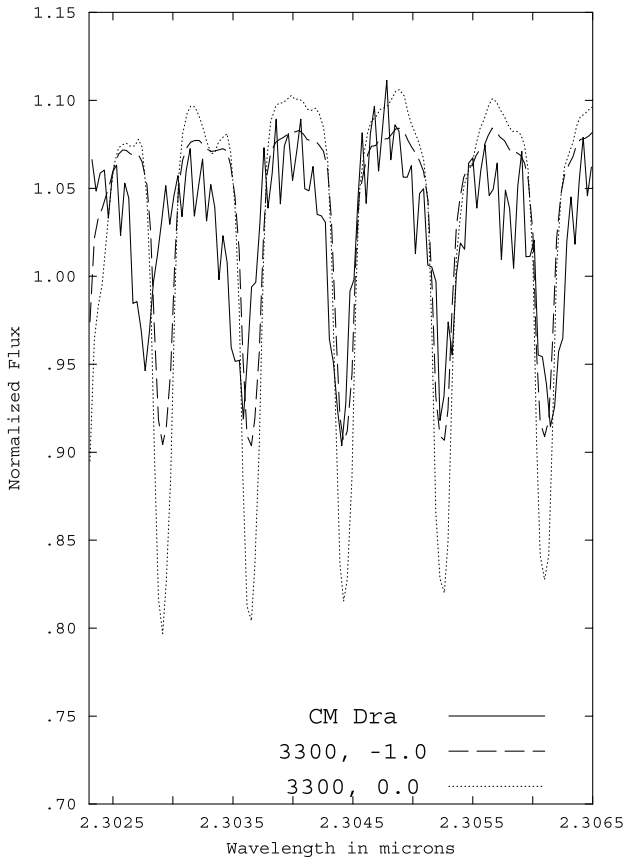

Figure 9. Carbon monoxide bands for CM Dra compared with synthetic spectra ($T_{\rm eff} = 3300$ K).

Both GJ 725B and GJ 699, unlike CM Dra, show other features next to some of the main CO features. For example, let us consider the strong CO blended feature centred at ∼2.3044 μm in the CM Dra spectrum; on its left-hand side a much weaker feature(s) may be present; this latter feature is stronger in GJ 699 and almost as strong as the one centred at ∼2.3044 μm in GJ 725B. In the synthetic spectra this feature is present, but it is weak and in fact not visible when we reduce the synthetic spectrum to the resolution of the observations. Moreover, by comparing the 'strong' CO feature centred at ∼2.3044 μm and its 'weak companion' in models computed at different temperatures and metallicities, we find they are not sensitive to either temperature or metallicity. The reliability of the CO linelist gives us confidence that any change in the strength of these two features due to varying the effective temperature would show. However, we also note that the quality of the observations for GJ 725B and GJ 699 is relatively poor. For GJ 725B, the region was observed at the very end of the second night of the observing run and for a very short integration time, and so the S/N is relatively poor; for GJ 699, observations were made during the third night when, in general, the weather conditions had worsened from previous nights. None the less, we have inter-compared the standards taken for each of the objects, and we do not find evidence for any changes in telluric features or differences in S/N which might be introduced by clouds. We therefore speculate on the possible cause of the double CO features.

From the atlas of dark sunspots (Wallace et al. 1996) and of Arcturus (Hinkle, Wallace & Livingston 1995) we do not find any evidence for double CO features. Although most of the CO bands observed are in fact combinations of two different $\Delta\nu = 2$ transitions (e.g., the 2.305-μm feature is made up of R27 and R74 transitions, separated by 0.0001 μm), the separation between the features is too small to be seen in these observations. The features might be due to companions to GJ 725B and GJ 699, but this seems unlikely. Apart from both having very similar radial velocities, not all CO features are doubled. The feature at 2.3036 is right on a telluric feature, and so the strength of this feature is not as reliable as the others. Indeed, in CM Dra this feature appears relatively stronger compared to GJ 699 and GJ 752B than might be expected from looking at other features. Another possibility is that the cores of the strong CO features are filled in, so that the lines appear as doublets. Given the substantial chromospheric activity of many M dwarfs (Delfosse et al. 1998), chromospheric emission might fill in the line cores. This would imply that the CO features are very much stronger in GJ 699 and GJ 752B, and the NLTE in-filling asymmetric in a similar manner. The canonical indicators of a strong chromosphere activity are substantial emission at Hα, X-ray and radio wavelengths. However, inspection of Hα (Leggett 1992), X-ray (Marino, Micela & Peres 2000) and radio (Wendker 1995) data does not indicate that GJ 699 and GJ 752B are particularly active relative to CM Dra.

The features might be atomic; certainly, the feature at 2.3059 μm is likely to be at least partly Ca, although there is no indication from the models or the sunspots and Arcturus atlases

that there are any other atomic features likely to play a significant role in this spectral region.

5 RESULTS

Based on a comparison of synthetic and observed spectra in the near-infrared region, we have investigated the metallicity of the binary system CM Dra, along with GJ 699 and GJ 725B. During the course of our analysis we found the following results.

(1) Weak atomic features in the spectra were not well matched by synthetic spectra.

(2) CO $\Delta\nu = 2$ bands are more sensitive to metallicity than effective temperature changes. Although for the purpose of this analysis we considered only effective temperatures varying from 3100 to 3300 K (representing the probable extremes of effective temperature of CM Dra), we have confirmed this result by comparing low-resolution synthetic spectra ($\Delta\lambda = 2$Å) down to 2600 K.

(3) CO $\Delta\nu = 2$ bands were well matched by the synthetic spectra, and indicate a metallicity of [M/H] ~ -1.0 for CM Dra. This result supports the infrared work of Viti et al. (1997), but does not agree with various evolutionary models or optical analyses.

(4) Many of the CO bands for GJ 699 and GJ 752B appeared as double features; the only viable explanation for these features seems to be infilling due to chromospheric emission. Further observations and modelling are required to clarify this result.

From these observations it is apparent that high-resolution observations of M dwarfs can provide a powerful tool for understanding their composition. In particular, the CO bands appear to be a very powerful tool in such analyses. Our results should be checked for a wider sample of M dwarfs at higher resolution and signal-to-noise ratio. They might also be extended so as to include the ^{13}CO 2–0 bands. Observations yielding the $^{12}C/^{13}C$ ratio as a chronometer would be a further check on the origin of CM Dra and other suspected metal-poor stars.

ACKNOWLEDGMENTS

We thank the staff at the United Kingdom Infrared Telescope for assistance with the observations.

REFERENCES

Allard F., Hauschildt P. H., Schwenke D., 2000, ApJ, 540, 1005
Baraffe I., Chabrier G., Allard F., Hauschildt P. H., 1997, A&A, 327, 1054
Baraffe I., Chabrier G., Allard F., Hauschildt P. H., 1998, A&A, 337, 403
Bessell M. S., 1982, Proc. Astron. Soc. Aust., 4, 417
Burrows A., Hubbard W. B., Saumon D., Lunine J. I., 1993, ApJ, 406, 158
Burrows A. et al., 1997, ApJ, 491, 856
Carbon D. F., Milkey R. W., Heasley J. N., 1976, ApJ, 207, 253
Delfosse X., Forveille T., Perrier C., Mayor M., 1998, A&A, 331, 581
Gizis J., 1997, AJ, 113, 806
Goorvitch D., 1994, ApJS, 95, 535
Hauschildt P. H., Allard F., Baron E., 1999, ApJ, 512, 377
Hinkle K., Wallace L., Livingston W., 1995, PASP, 107, 1042
Horne K., 1986, PASP, 98, 609
Jones H. R. A., Longmore A. J., Allard F., Hauschildt P. H., 1996, MNRAS, 280, 77
Kraus M., Hrügel E., Thum C., Geballe T. R., 2000, A&A, 362, 158
Lacy C. H., 1977, ApJ, 218, 444
Leggett S. K., 1992, ApJS, 82, 351
Leggett S. K., Allard F., Hauschildt P. H., 1998, ApJ, 509, 836
Marino A., Micela G., Peres G., 2000, A&A, 353, 177
Metcalfe T. S., Mathieu R. D., Latham D. W., Torres G., 1996, ApJ, 456, 356
Montalbán J., D'Antona F., Mazzitelli I., 2000, A&A, 360, 935
Paczyński B., Sienkiewicz R., 1984, ApJ, 286, 332
Rucinski S. M., 1978, Acta Astron., 28, 167
Tsuji T., 1977, PASJ, 29, 497
Tsuji T., 1986, A&A, 156, 8
Tsuji T., 1991, A&A, 245, 203
Valenti J. A., Piskunov N., Johns-Krull C. M., 1998, ApJ, 498, 851
Viti S., Jones H. R. A., 1999, A&A, 351, 1028
Viti S. et al., 1997, MNRAS, 291, 780
Wallace L., Livingston W., Hinkle K., Bernath P., 1996, ApJS, 106, 165
Wendker H. J., 1995, A&AS, 109, 177

This paper has been typeset from a TEX/LATEX file prepared by the author.